

# The magnetic signatures of the $M_2$ , $N_2$ and $O_1$ oceanic tides observed in Swarm and CHAMP satellite magnetic data

Alexander V. Grayver<sup>1</sup>, Nils Olsen<sup>2</sup>

<sup>1</sup>Institute of Geophysics, ETH Zürich, Switzerland.

<sup>2</sup>DTU Space, Technical University of Denmark, Denmark

## Key Points:

- Global models of the magnetic signals produced by the  $M_2$ ,  $N_2$ ,  $O_1$  oceanic tides have been extracted from satellite magnetic measurements
- Combining data from the Swarm and CHAMP missions as well as using field gradient play key role in the robustness of the estimated models
- All tidal constituents show significant sensitivity to the electrical conductivity of the oceanic mantle

13 **Abstract**

14 This paper reports on new results in the determination of magnetic signals produced by  
 15 oceanic tides as determined from satellite magnetic measurements. We find that combining  
 16 data from the past CHAMP (2000 – 2010) and the present Swarm (since 2013) satel-  
 17 lite missions significantly improves the quality of the extracted tidal signals, in particular  
 18 if along-track and cross-track magnetic “gradient” data are utilized. This allows us to de-  
 19 termine the magnetic signature not only of the  $M_2$  tide but also of the much weaker  $N_2$   
 20 and  $O_1$  tidal constituents. To minimize disturbances from magnetospheric and ionospheric  
 21 currents, we only use data from the nightside region during geomagnetic quiet conditions,  
 22 and remove core, crustal and magnetospheric field contributions as given by the CHAOS  
 23 geomagnetic field model. Despite their small magnitudes, all determined tidal constituents  
 24 show sensitivity to the electrical conductivity profile of the underlying mantle, enabling  
 25 imaging the upper mantle below the oceans.

26 **1 Introduction**

27 Tidal motion of the electrically conducting seawater in the oceans produce a mag-  
 28 netic field signature by means of a phenomena called motional induction [Sanford, 1971;  
 29 Chave and Luther, 1990; Tyler *et al.*, 1997]. The first successful attempt to globally de-  
 30 termine the weak magnetic tidal signal (of the strongest lunar tidal constituent,  $M_2$ ) used  
 31 two years of magnetic observations taken by the CHAMP satellite mission [Tyler *et al.*,  
 32 2003]. This work demonstrated the remarkable high quality of satellite magnetic data and  
 33 envisaged some applications of the determined  $M_2$  signal, although these applications were  
 34 hindered by insufficient quality of the magnetic tidal determination at that time. This has  
 35 changed with the release of the “Comprehensive Model 5” (CM5) [Sabaka *et al.*, 2015],  
 36 which, among others, resulted in a substantially improved quality of the extracted  $M_2$   
 37 magnetic tidal signal, enabling its use for probing the electrical conductivity of the up-  
 38 per mantle beneath the oceans [Schnepp *et al.*, 2015; Grayver *et al.*, 2016]. These papers  
 39 demonstrated feasibility of using satellite-detected magnetic tidal signals as an electromag-  
 40 netic induction source for imaging the upper mantle below the oceans on a global scale,  
 41 complementing previous attempts based on local measurements of tidal EM signals for  
 42 conductivity sounding [e.g. Larsen, 1968; Kuvshinov *et al.*, 2006]. This source aims at  
 43 complementing marine magnetotellurics [e.g. Evans *et al.*, 2005; Naif *et al.*, 2013], an al-  
 44 ternative method to study oceanic upper mantle, but with some limitations due to its high  
 45 cost and inherent logistical challenges. Therefore, a successful determination of tidal con-  
 46 stituents other than the dominant  $M_2$  mode, and improving overall quality, will lead to  
 47 better constrained electrical structure of the oceanic mantle. Furthermore, also other appli-  
 48 cations like remote sensing of the ocean dynamics also will benefit from improved models  
 49 of tidal magnetic signals [e.g. Minami, 2017; Saynisch *et al.*, 2017; Trossman and Tyler,  
 50 2019].

51 The CM5 magnetic field model is based on magnetic data taken by the pre-Swarm  
 52 satellite missions Ørsted, CHAMP, and SAC-C. Although these missions all consist of a  
 53 single satellite, the data set includes a particularly favourable period between 2007 and  
 54 2010 when CHAMP was flying at low altitudes during a solar minimum. In contrast, the  
 55 three-satellite constellation mission Swarm (in operation since November 2013) enables  
 56 measuring the East-West (mainly cross-track) magnetic field gradient (approximated in  
 57 practice by finite differences of simultaneous observations taken by the side-by-side fly-  
 58 ing satellites Swarm Alpha and Charlie), in addition to the along-track gradient (approxi-  
 59 mated by finite differences of succeeding measurements taken by a single satellite). This  
 60 results in an improved determination of the  $M_2$  signal [Sabaka *et al.*, 2016, 2018] despite  
 61 the higher solar activity and altitude as compared to CHAMP. So far, the combined analy-  
 62 sis of both CHAMP and Swarm data for tidal signals has not been reported. Furthermore,  
 63 most studies use the “Comprehensive Inversion” approach (CI), which strives for a consis-  
 64 tent co-estimation of various magnetic field sources by accounting for various dependen-

65 cies and correlations of the data and modelled sources. However, the comprehensive in-  
 66 version approach is very resource and time demanding and thus sub-optimal for hypothesis  
 67 testing and optimal parameter search. A sequential approach, focusing on determination  
 68 of tidal signals from magnetic field residuals (i.e. observations minus model predictions  
 69 of non-tidal fields like core and crustal field contributions) is much faster and thus better  
 70 suited for parameter optimisation experiments.

71 Global determination of tidal constituents other than  $M_2$  is challenging due to the  
 72 much smaller amplitudes, although some promising results have been obtained in regions  
 73 where the signals are strong [e.g. *Maus and Kuvshinov*, 2004; *Sabaka et al.*, 2016]. Con-  
 74 stituents other than  $M_2$  would provide additional constraints on the mantle conductivity in  
 75 regions where  $M_2$  is weak. Further, even though some constituents may have very similar  
 76 periods (for instance,  $M_2$  and  $N_2$ ), their flows and hence generated electric currents dif-  
 77 fer, thus leading to unique sensitivity footprints. The latter property may be particularly  
 78 advantageous for exploring lateral conductivity heterogeneities in the mantle.

79 Motivated by these arguments, current study aims at extracting magnetic signatures  
 80 of the three tidal constituents  $M_2$ ,  $N_2$  and  $O_1$  by joint analysis of CHAMP and Swarm  
 81 satellite magnetic data. Because of its simplicity and speed, we adopt the sequential ap-  
 82 proach which enables a systematic testing of various model parametrizations and data se-  
 83 lection criteria.

## 84 2 Methodology

### 85 2.1 Data selection

86 The analysis is based on magnetic field observations taken by the CHAMP and  
 87 Swarm satellites. CHAMP data between 2000 and 2010 and Swarm data between Novem-  
 88 ber 2013 and September 2018 were used. We do not include any ground magnetic ob-  
 89 servatory data and rely solely on satellite measurements. The data selection criteria are  
 90 identical to those used for deriving the CHAOS-6 model [*Finlay et al.*, 2016] with the only  
 91 exception that we exclude any dayside data and thus only work with data from the dark  
 92 side (sun at least  $10^\circ$  below the horizon). This is done to minimize the effects of the lunar  
 93 ionospheric tidal signals, which contaminate oceanic signals on the day side [e.g. *Malin*  
 94 and *Chapman*, 1970; *Olsen*, 1997; *Alken and Maus*, 2007; *Schnepf et al.*, 2018]. Both vec-  
 95 tor and scalar fields and their along- and cross-track differences are used (see *Finlay et al.*  
 96 [2016] for details), resulting in  $3 \times 1,174,834$  vector data,  $3 \times 799,337$  vector differences,  
 97 326,417 scalar data and 1,534,374 scalar differences distributed in time as shown in Fig-  
 98 ure 1. Following *Finlay et al.* [2016], we use scalar data only poleward of the  $\pm 55^\circ$  quasi-  
 99 dipole (QD) latitude, resulting in a relatively small amount of scalar field observations.

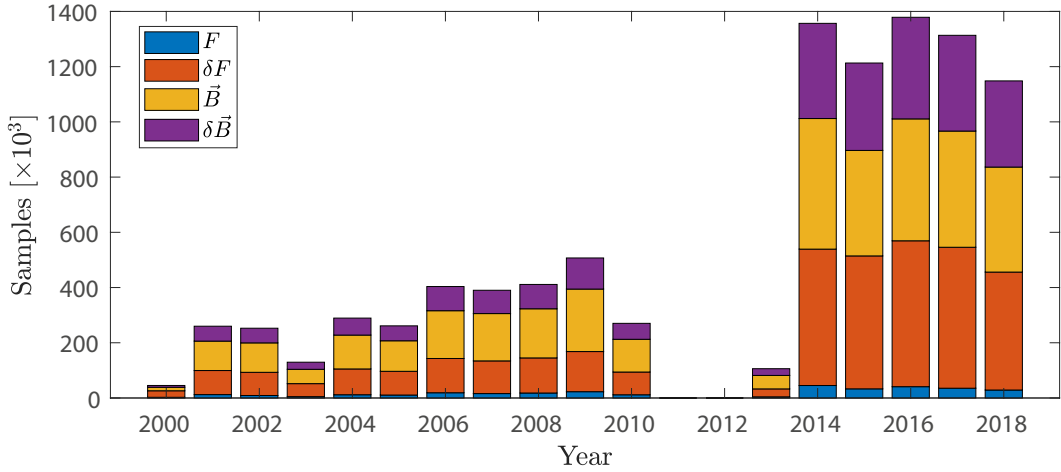
103 To account for the core, lithosphere and large-scale magnetospheric components,  
 104 we subtract from the observations model predictions of these three sources as given by  
 105 the CHAOS-6 model (version x7). The obtained residuals comprise the input data for this  
 106 study.

### 107 2.2 Signal extraction

108 Our model parametrization follows *Sabaka et al.* [2018]: the magnetic signal  $\vec{B} =$   
 109  $-\nabla V(t, \vec{r})$  of tides is represented by a magnetic scalar potential  $V$ . At time  $t$  and position  
 110  $\vec{r}$ ,  $V$  is expanded via spherical harmonics as

$$111 V(t, \vec{r}) = \text{Re} \left\{ \exp(i\omega t) R_E \sum_{n=1}^{N_{\max}} \left( \frac{R_E}{r} \right)^{n+1} \sum_{m=-n}^n \tau_n^m P_n^{|m|}(\cos \theta) \exp(im\phi) \right\}, \quad (1)$$

111 where  $R_E = 6371.2$  km is Earth's mean radius;  $\vec{r} = (r, \theta, \phi)$  is the position vector with  
 112  $\phi, \theta$  being geographic longitude and co-latitude, respectively;  $\tau_n^m$  are complex spherical



100 **Figure 1.** Time distribution of the satellite data used in this study. Period prior to 2011 corresponds to the  
 101 CHAMP satellite data while period after 2013 to the Swarm phase. Symbols  $F, \delta F, \vec{B}, \delta \vec{B}$  denote scalar,  
 102 scalar difference, vector and vector difference data, respectively.

120 **Table 1.** Tidal constituents, their period  $T$  and maximum spherical harmonic degree  $N_{\max}$  used in the model  
 121 parametrization.

Constituent	$T$ (hours)	$N_{\max}$
$M_2$	12.4206	28
$N_2$	12.6583	12
$O_1$	25.8193	12

113 harmonic coefficients of spherical harmonic degree  $n$  and order  $m$ ;  $P_n^{[m]}$  are Schmidt-  
 114 normalized Legendre functions; angular frequencies  $\omega = 2\pi/T$  with  $T$  being the period  
 115 of a tidal constituent; and  $\text{Re}(\cdot)$  denotes the real part. Different tidal constituents are es-  
 116 timated separately using the period  $T$  and maximum spherical harmonic degree  $N_{\max}$  as  
 117 listed in Table 1.  $N_{\max}$  is chosen based on numerous trials as a trade-off between low  
 118 noise levels and high spatial resolution. More data in the future will likely enable higher  
 119 resolution of the extracted signals without compromising quality.

122 We use robust linear regression (iteratively re-weighted least squares (IRLS) [Aster  
 123 *et al.*, 2018] with Huber weights [Constable, 1988]) to estimate the spherical harmonic  
 124 coefficients  $\tau_n^m$  for each of the three tidal constituents. This robust approach is similar to  
 125 the one described e.g. in [Olsen *et al.*, 2017] with some modifications explained in the  
 126 “Supporting Information”.

127 Following previous studies, the spatial power spectrum at altitude corresponding to  
 128 radius  $r$  is defined as

$$R_n(r) = \frac{n+1}{2} \left( \frac{R_E}{r} \right)^{2n+4} \left[ |\tau_n^0|^2 + \sum_{m=1}^n \left( |\tau_n^m|^2 + |\tau_n^{-m}|^2 \right) \right]. \quad (2)$$

### 129 2.3 Forward modelling of tidal magnetic signals

130 In order to compare the estimated tidal signals with theoretical values, we performed  
 131 numerical simulations using the radial mantle conductivity profile of Grayver *et al.* [2017]

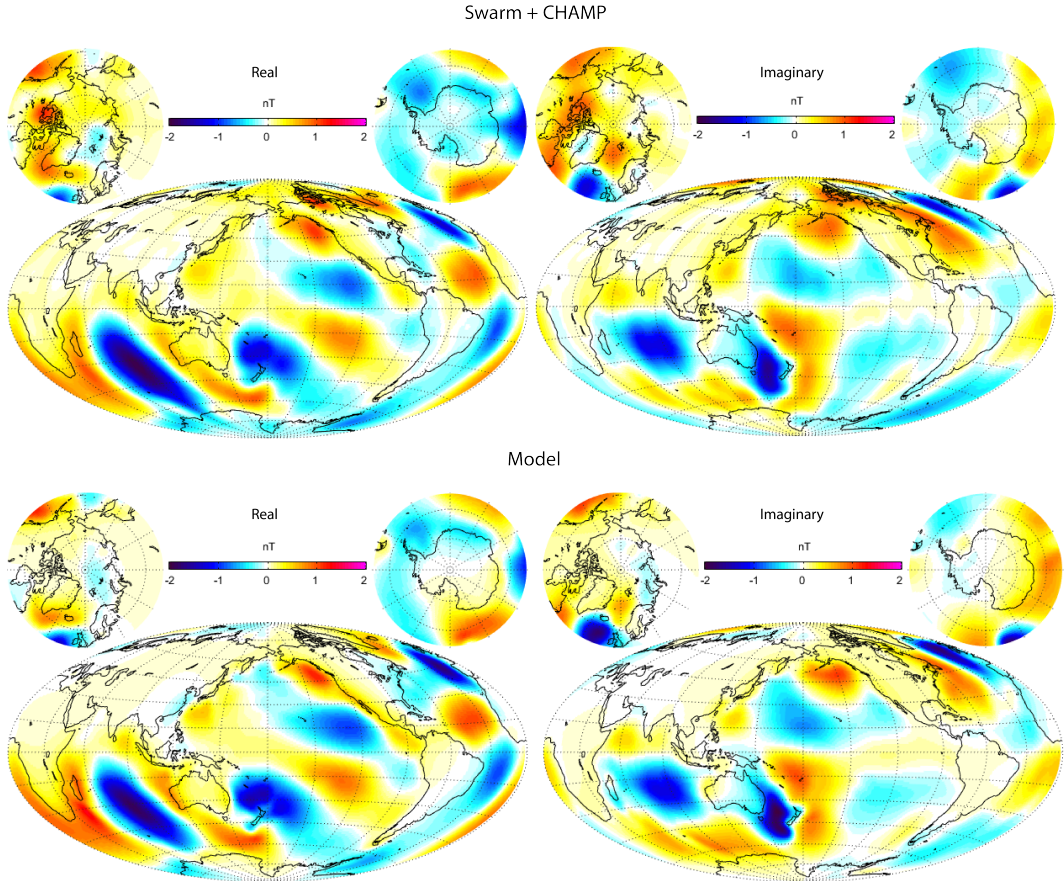


**Figure 2.** Estimated (top) and simulated (bottom) magnetic radial component due to the  $M_2$  tide. Shown are real (left) and imaginary (right) parts of the signal at 430 km altitude.

overlaid by a shell with heterogeneous conductivities representing the ocean and sediments [Manoj *et al.*, 2006]. The electrical current source  $\mathbf{u} \times \mathbf{B}_0$  is given by the TPXO9 model [Egbert and Erofeeva, 2002] of tidal transport  $\mathbf{u}$  and the IGRF-12 magnetic field model [Thébault *et al.*, 2015] for the ambient magnetic field  $\mathbf{B}_0$ . We solve the full Maxwell's equations using a finite-element global electromagnetic solver [Grayver *et al.*, 2019] based on several open-source libraries [Alzetta *et al.*, 2018; Balay *et al.*, 2018; Karypis and Kumar, 1999]. In simulations, the ocean is galvanically coupled to the mantle, resulting in a bi-modal induced fields [Chave and Luther, 1990; Velimsky *et al.*, 2018]. In the study case of an insulating mantle, a conductivity of  $10^{-7}$  S/m is formally assigned.

### 3 Results

Figures 2 to 4 compare observed (top) and modelled (bottom) radial magnetic field components for each of the three tidal constituents analysed in this study. The dominant  $M_2$  tide (Figure 2) produces magnetic signals up to 2 nT at 430 km altitude and reveals, similar to previous studies, an observed signals (top) that is in remarkably good agreement with the simulated fields (bottom). However, the fascinating and novel outcome of this study is that we additionally determined globally the much weaker  $N_2$  (Figure 3) and  $O_1$  (Figure 4) magnetic signals. The amplitudes of these signals hardly reach 0.5 nT at satellite altitudes, yet the agreement with the simulation results is very good, particularly at middle and low latitudes. The larger discrepancy at polar latitudes originates likely from

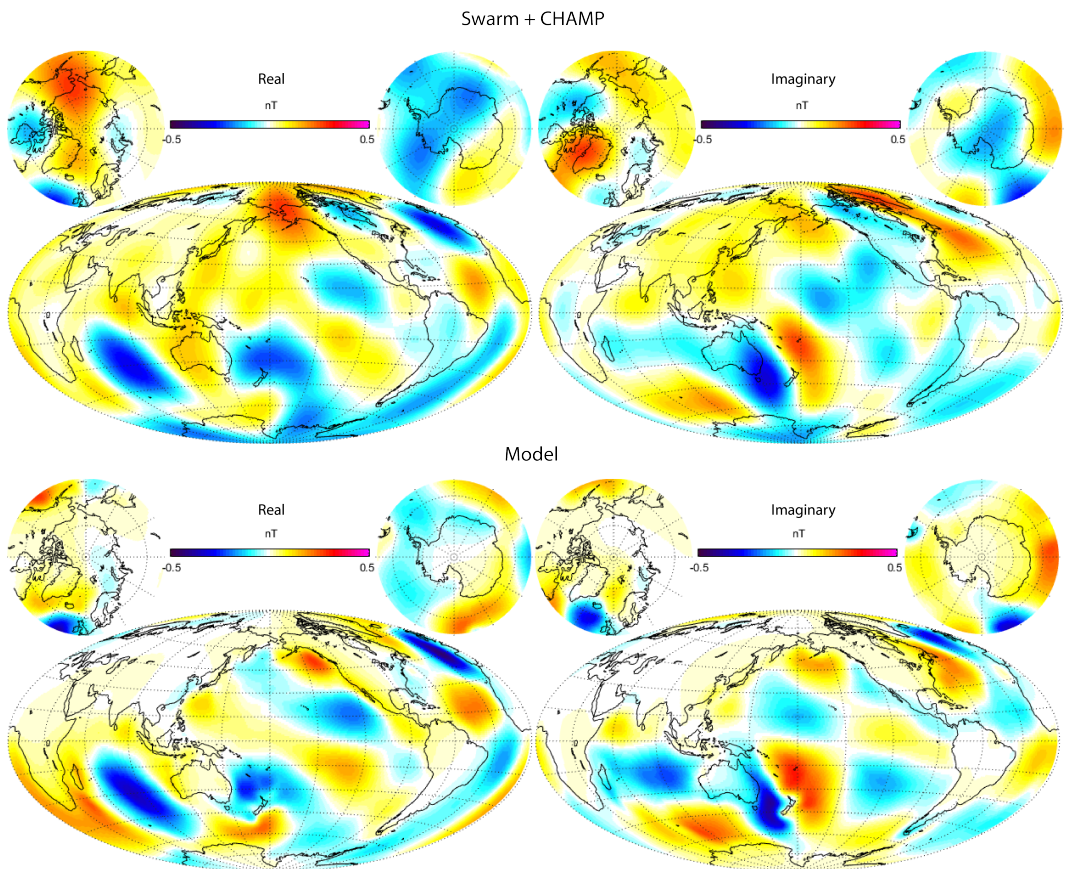
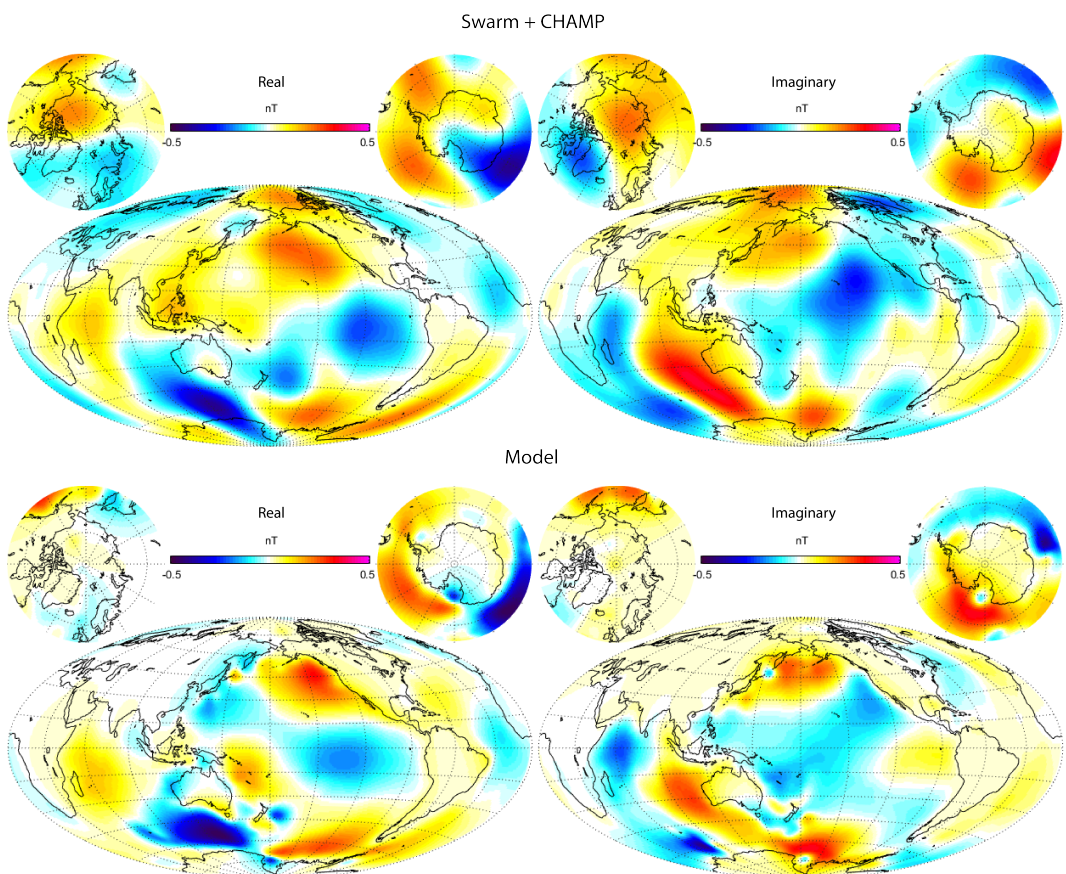


**Figure 3.** Same as Figure 2, but for the  $N_2$  tide.



145

**Figure 4.** Same as Figure 2, but for the  $O_1$  tide.

155 contamination by ionospheric polar currents, which we do not account for in this study.  
 156 Nevertheless, the contaminant signals are on the order of 0.1 – 0.2 nT and remain accept-  
 157 able.

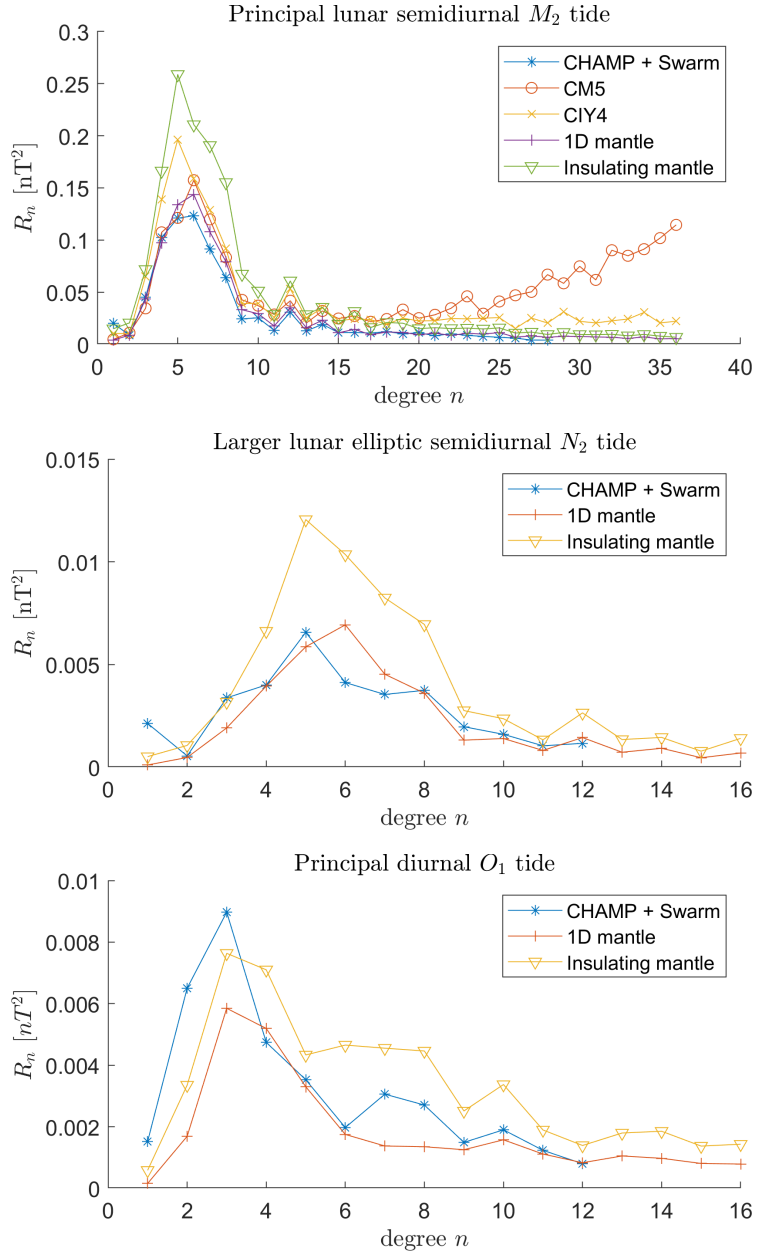
164 Spatial power spectra  $R_n$  (eq. 2) of the observed magnetic tidal fields are shown in  
 165 Figure 5. For reference, we also show spectra of the simulated signals for an insulating,  
 166 respectively electrically conductive, mantle. Their difference demonstrate that all tidal con-  
 167 stituents, including the weaker  $N_2$  and  $O_1$  constituents, exhibit sensitivity to the electri-  
 168 cal conductivity of the underlying mantle: the spectra of the observed field follow more  
 169 closely those of the simulated signals for a conducting mantle. An insulating mantle pro-  
 170 duces much stronger magnetic signals due to the absence of attenuation in the mantle.  
 171 Despite this model likely does not represent reality, it gives an upper bound on the noise  
 172 level, hence providing an objective criterion for evaluating the quality of the extracted sig-  
 173 nal. For instance, the low-degree ( $n = 1 – 3$ ) part of the  $O_1$  spectrum, where the obser-  
 174 vations are higher than the insulating mantle spectrum, might be contaminated by fields of  
 175 magnetospheric origin and thus should be interpreted with care.

180 In order to study the key aspects which enable the extraction of the weak  $N_2$  and  
 181  $O_1$  tidal signals, we now investigate the effect of combining CHAMP and Swarm satellite  
 182 data, as well as the role of field difference (“gradient”) data. Figure 6, top row shows spa-  
 183 tial spectra for signals obtained by analysing CHAMP, respectively Swarm, data separately  
 184 and jointly. Clearly, combining data from both satellite missions significantly improves the  
 185 signal-to-noise ratio and stabilizes the obtained solution. Further, Figure 6, bottom row  
 186 shows the effect of using different data types. It is clear that excluding field difference  
 187 (“gradient”) data and working only with field data leads to less reliable solutions, espe-  
 188 cially for spherical harmonic degrees  $n > 5$ , where gradients likely help suppress contam-  
 189 ination by unmodelled (probably ionospheric and magnetospheric) contributions. On the  
 190 other hand, excluding field data and relying only on the field differences results in a very  
 191 unstable model. This finding is different from the experience in lithospheric modelling  
 192 [e.g. Kotsiaros *et al.*, 2014; Olsen *et al.*, 2017] where very good results were obtained from  
 193 an analysis of gradient data alone, probably due to the smaller spatial scale of the litho-  
 194 spheric field which favours gradient information. In contrast, for the determination of  
 195 the magnetic signature of oceanic tides the gradient data play an important role, but the  
 196 inclusion of field data remains crucial.

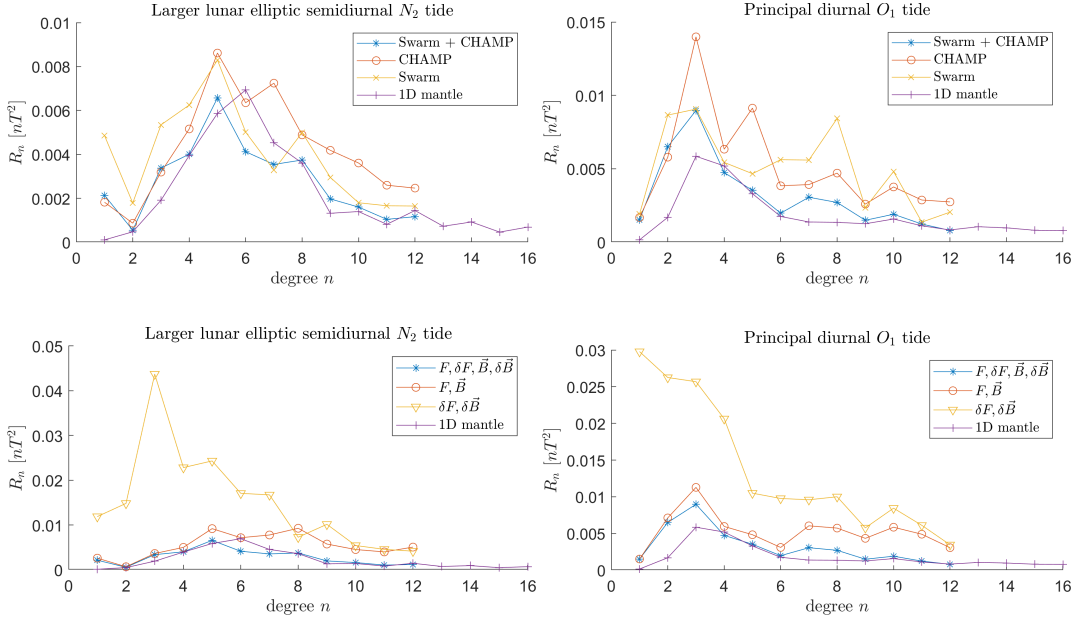
197 Animations of the time-dependence of the tidal signals for all constituents are given  
 198 in the supplementary material.

### 199 3.1 Implications for conductivity of oceanic mantle

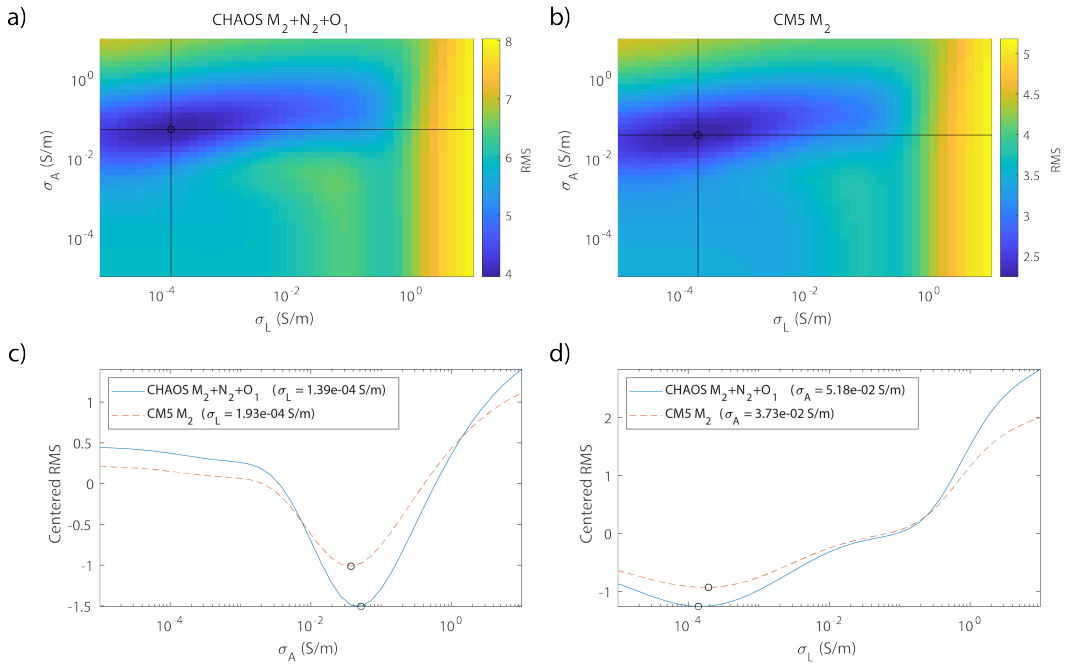
204 We tested the sensitivity of both the new and previously extracted signals to the con-  
 205 ductivity values of the lithosphere and asthenosphere by means of a two-parameter model.  
 206 Assuming an average oceanic lithosphere thickness of 70 km [Rychert and Shearer, 2009],  
 207 we varied the conductivity values of the two layers and calculated the root-mean-square  
 208 (RMS) error between the calculated and observed radial magnetic field components at  
 209 satellite altitude (430 km). We used tidal signals obtained in this study and the  $M_2$  signal  
 210 from the CM5 model [Sabaka *et al.*, 2015]. Errors derived from the formal posterior co-  
 211 variance matrix [Aster *et al.*, 2018] were used to normalize the misfit. Figure 7(a,b) shows  
 212 the RMS as a function of the lithosphere and asthenosphere conductivity. Although the ab-  
 213 solute RMS error depends on the data uncertainty, the slopes and location of the minimum  
 214 in the plots characterize the sensitivity and the most probable solution, respectively. Fig-  
 215 ure 7(c,d) show centred RMS profiles for the best fit parameters. First of all, one sees a  
 216 good agreement between the most probable solutions from CM5 and present study signals,  
 217 which shows the high quality of CM5, but also confirms that the approach adopted here  
 218 provides reliable estimates. The current tidal signals suggest a slightly more conductive  
 219 asthenosphere and a more resistive lithosphere. While this is favoured by laboratory con-



158 **Figure 5.** Spatial power spectra  $R_n$  of the extracted and simulated tidal signals at Earth's surface. Top:  
159  $M_2$  spectra from this study (denoted as “CHAMP + Swarm”) and spectra obtained in previous studies (CM5  
160 denotes “Comprehensive Model 5” [Sabaka *et al.*, 2015] and CIY4 denotes “Comprehensive Inversion Year  
161 4”) [Sabaka *et al.*, 2018]. For reference, spectra of the simulated fields based on a 1D conductivity profile and  
162 an insulating mantle, respectively, are given (see Section 2.3). Middle and Bottom: same as top, but for the  
163  $N_2$  and  $O_1$  tidal constituents, respectively.



176 **Figure 6.** Spatial power spectra of the  $N_2$  and  $O_1$  signals at Earth's surface. Top row: signals estimated  
 177 from either CHAMP or Swarm data as well as using data from both missions. Bottom row: signals esti-  
 178 mated using either field data or field difference ("gradient") data, as well as using both of them. For reference,  
 179 spectra of the modelled fields using a 1D mantle conductivity profile are given.



200 **Figure 7.** (a,b) Root-mean-square (RMS) error between simulated and observed signals for various con-  
 201 ductivity values of the astenosphere ( $\sigma_A$ ) and a 70 km thick lithosphere ( $\sigma_L$ ). Black circles indicate the position  
 202 of the minimum. (c,d) Graphs of the centred RMS values along black lines shown in (a,b). Legend items  
 203 show conductivity values of the corresponding conditional variable.

ductivity profiles [Grayver *et al.*, 2017], the differences may lie within the uncertainty and should be confirmed with future additional data. Additionally, steep slopes for the present signals indicate higher sensitivity to the conductivity variations in the mantle.

## 4 Conclusions

We provide the first global observation of the magnetic signatures generated by the  $N_2$  and  $O_1$  oceanic tides, based on a combined analysis of 10 years of CHAMP and almost 5 years of Swarm satellite magnetic data. Along-track and cross-track field difference (“gradient”) data play a key role in obtaining robust estimates at smaller spatial scales. Additional forthcoming data from Swarm may potentially make an extraction of even weaker tidal constituents feasible. As we enter a period of low solar activity, and the Swarm satellite altitude naturally descend, new data are likely to further increase the quality of the obtained models, hence refining our knowledge about oceanic mantle.

## Acknowledgments

We thank ESA for rapid and easy access to the Swarm Level 1b data, which are available from ESA at <http://earth.esa.int/swarm>. The support of the CHAMP mission by the German Aerospace Center (DLR) and the Federal Ministry of Education and Research is gratefully acknowledged. This work was supported by ESA through the Swarm DISC project. Spherical harmonic expansion coefficients of the estimated tidal signals are available in the “Supporting Information”. We thank Alexey Kuvshinov, Chris Finlay and Lars Tøffner-Clausen for insightful discussions on the data processing and modeling.

## References

- Alken, P., and S. Maus (2007), Spatio-temporal characterization of the equatorial electrojet from champ, ørsted, and sac-c satellite magnetic measurements, *Journal of Geophysical Research: Space Physics*, 112(A9).
- Alzetta, G., D. Arndt, W. Bangerth, V. Boddu, B. Brands, D. Davydov, R. Gassmøller, T. Heister, L. Heltai, K. Kormann, et al. (2018), The deal. ii library, version 9.0, *Journal of Numerical Mathematics*, 26(4), 173–183.
- Aster, R. C., B. Borchers, and C. H. Thurber (2018), *Parameter estimation and inverse problems*, Elsevier.
- Balay, S., S. Abhyankar, M. F. Adams, J. Brown, P. Brune, K. Buschelman, L. Dal-cin, A. Dener, V. Eijkhout, W. D. Gropp, D. Kaushik, M. G. Knepley, D. A. May, L. C. McInnes, R. T. Mills, T. Munson, K. Rupp, P. Sanan, B. F. Smith, S. Zampini, H. Zhang, and H. Zhang (2018), PETSc users manual, *Tech. Rep. ANL-95/11 - Revision 3.10*, Argonne National Laboratory.
- Chave, A. D., and D. S. Luther (1990), Low-frequency, motionally induced electromagnetic fields in the ocean. 1. Theory., *Journal of Geophysical Research*, 95, 7185–7200.
- Constable, C. (1988), Parameter estimation in non-gaussian noise, *Geophysical Journal*, 94(1), 131–142.
- Egbert, G. D., and S. Y. Erofeeva (2002), Efficient inverse modeling of barotropic ocean tides, *Journal of Atmospheric and Oceanic Technology*, 19(2), 183–204.
- Evans, R. L., G. Hirth, K. Baba, D. Forsyth, A. Chave, and R. Mackie (2005), Geophysical evidence from the MELT area for compositional controls on oceanic plates, *Nature*, 437(7056), 249–252.
- Finlay, C. C., N. Olsen, S. Kotsiaros, N. Gillet, and L. Tøffner-Clausen (2016), Recent geomagnetic secular variation from swarm and ground observatories as estimated in the CHAOS-6 geomagnetic field model, *Earth, Planets and Space*, 68(1), 112.
- Grayver, A. V., N. R. Schepf, A. V. Kuvshinov, T. J. Sabaka, C. Manoj, and N. Olsen (2016), Satellite tidal magnetic signals constrain oceanic lithosphere-asthenosphere

- boundary, *Science Advances*, 2(9), e1600,798.
- Grayver, A. V., F. D. Munch, A. V. Kuvshinov, A. Khan, T. J. Sabaka, and L. Tøffner-Clausen (2017), Joint inversion of satellite-detected tidal and magnetospheric signals constrains electrical conductivity and water content of the upper mantle and transition zone, *Geophysical research letters*, 44(12), 6074–6081.
- Grayver, A. V., M. van Driel, and A. V. Kuvshinov (2019), Three-dimensional magnetotelluric modeling in spherical earth, *Geophysical Journal International*.
- Karypis, G., and V. Kumar (1999), A fast and highly quality multilevel scheme for partitioning irregular graphs, *Journal on Scientific Computing*, 20(1), 359–392.
- Kotsiaros, S., C. Finlay, and N. Olsen (2014), Use of along-track magnetic field differences in lithospheric field modelling, *Geophysical Journal International*, 200(2), 880–889.
- Kuvshinov, A., A. Junge, and H. Utada (2006), 3-D modelling the electric field due to ocean tidal flow and comparison with observations, *Geophysical research letters*, 33(6).
- Larsen, J. (1968), Electric and magnetic fields induced by deep sea tides, *Geophysical Journal of the Royal Astronomical Society*, 16(1), 47–70.
- Malin, S., and S. Chapman (1970), Lunar tidal components N2 and O1 in the atmospheric pressure, *pure and applied geophysics*, 80(1), 309–318.
- Manoj, C., A. Kuvshinov, S. Maus, and H. Lühr (2006), Ocean circulation generated magnetic signals, *Earth, Planets and Space*, 58(4), 429–437.
- Maus, S., and A. Kuvshinov (2004), Ocean tidal signals in observatory and satellite magnetic measurements, *Geophysical Research Letters*, 31(15).
- Minami, T. (2017), Motional induction by tsunamis and ocean tides: 10 years of progress, *Surveys in Geophysics*, 38(5), 1097–1132.
- Naif, S., K. Key, S. Constable, and R. Evans (2013), Melt-rich channel observed at the lithosphere-asthenosphere boundary, *Nature*, 495(7441), 356–359.
- Olsen, N. (1997), Geomagnetic tides and related phenomena, in *Tidal Phenomena*, pp. 261–274, Springer.
- Olsen, N., D. Ravat, C. C. Finlay, and L. K. Kother (2017), LCS-1: a high-resolution global model of the lithospheric magnetic field derived from CHAMP and Swarm satellite observations, *Geophysical Journal International*, 211(3), 1461–1477.
- Rychert, C. A., and P. M. Shearer (2009), A global view of the lithosphere-asthenosphere boundary, *Science*, 324(5926), 495–498.
- Sabaka, T. J., N. Olsen, R. H. Tyler, and A. Kuvshinov (2015), CM5, a pre-Swarm comprehensive geomagnetic field model derived from over 12 yr of CHAMP, Ørsted, SAC-C and observatory data, *Geophysical Journal International*, 200(3), 1596–1626.
- Sabaka, T. J., R. H. Tyler, and N. Olsen (2016), Extracting ocean-generated tidal magnetic signals from swarm data through satellite gradiometry, *Geophysical Research Letters*, 43(7), 3237–3245.
- Sabaka, T. J., L. Tøffner-Clausen, N. Olsen, and C. C. Finlay (2018), A comprehensive model of Earth's magnetic field determined from 4 years of swarm satellite observations, *Earth, Planets and Space*, 70(1), 130.
- Sanford, T. B. (1971), Motionally induced electric and magnetic fields in the sea, *Journal of Geophysical Research*, 76(15), 3476–3492.
- Saynisch, J., J. Petereit, C. Irrgang, and M. Thomas (2017), Impact of oceanic warming on electromagnetic oceanic tidal signals: A CMIP5 climate model-based sensitivity study, *Geophysical Research Letters*, 44(10), 4994–5000.
- Schnepf, N., A. Kuvshinov, and T. Sabaka (2015), Can we probe the conductivity of the lithosphere and upper mantle using satellite tidal magnetic signals?, *Geophysical Research Letters*, 42(9), 3233–3239.
- Schnepf, N. R., M. Nair, A. Maute, N. M. Pedatella, A. Kuvshinov, and A. D. Richmond (2018), A comparison of model-based ionospheric and ocean tidal magnetic signals with observatory data, *Geophysical Research Letters*, 45(15), 7257–7267.

- 321 Thébault, E., C. C. Finlay, C. D. Beggan, P. Alken, J. Aubert, O. Barrois, F. Bertrand,  
322 T. Bondar, A. Boness, L. Brocco, et al. (2015), International geomagnetic reference  
323 field: the 12th generation, *Earth, Planets and Space*, 67(1), 79.
- 324 Trossman, D., and R. Tyler (2019), Predictability of ocean heat content from electrical  
325 conductance, *Journal of Geophysical Research: Oceans*.
- 326 Tyler, R. H., L. A. Mysak, and J. M. Oberhuber (1997), Electromagnetic fields gener-  
327 ated by a three dimensional global ocean circulation, *Journal of Geophysical Research*,  
328 102(C3), 5531–5551.
- 329 Tyler, R. H., S. Maus, and H. Lühr (2003), Satellite observations of magnetic fields due to  
330 ocean tidal flow, *Science*, 299(5604), 239–241.
- 331 Velímský, J., A. Grayver, A. Kuvshinov, and L. Šachl (2018), On the modelling of M2  
332 tidal magnetic signatures: effects of physical approximations and numerical resolution,  
333 *Earth, Planets and Space*, 70(1), 192.